ADVANCED FUNCTIONAL MATERIALS
www.afm-journal.de

Self-Healing, Flexible, and Tailorable Triboelectric Nanogenerators for Self-Powered Sensors based on Thermal Effect of Infrared Radiation

Xingyi Dai, Long-Biao Huang, Yuzhang Du, Jiancheng Han, Qiuqun Zheng, Jie Kong,* and Jianhua Hao**

Self-healing triboelectric nanogenerators (TENGs) with flexibility, robustness, and conformability are highly desirable for promising flexible and wearable devices, which can serve as a durable, stable, and renewable power supply, as well as a self-powered sensor. Herein, an entirely self-healing, flexible, and tailorable TENG is designed as a wearable sensor to monitor human motion, with infrared radiation from skin to promote self-healing after being broken based on thermal effect of infrared radiation. Human skin is a natural infrared radiation emitter, providing favorable conditions for the device to function efficiently. The reversible imine bonds and quadruple hydrogen bonding (UPy) moieties are introduced into polymer networks to construct self-healable electrification layer. UPy-functionalized multiwalled carbon nanotubes are further incorporated into healable polymer to obtain conductive nanocomposite. Driven by the dynamic bonds, the designed and synthesized materials show excellent intrinsic self-healing and shape-tailorable features. Moreover, there is a robust interface bonding in the TENG devices due to the similar healable networks between electrification layer and electrode. The output electric performances of the self-healable TENG devices can almost restore their original state when the damage of the devices occurs. This work presents a novel strategy for flexible devices, contributing to future sustainable energy and wearable electronics.

1. Introduction

Self-powered devices, as an emerging field, which are capable of converting surrounding energy into electrical energy, have shown great potential in various applications including artificial skins, sensors, nanorobotics, and portable/wearable devices.[1–5] Compared to the electronic devices driven by conventional power sources such as batteries and capacitor with the restrictions of bulky volume, limited lifetime, and environmental unfriendliness, the self-powered devices exhibit vast excellence. Recently, triboelectric nanogenerators (TENGs) as a green and sustainable power source have derived great attentions due to their merits, including wide material availability, diversified designability, low cost, and easy fabrication.[6–8] Based on the synergistic effect of contact electrification and electrostatic induction between different triboelectric materials, TENGs could be effectively utilized to harvest mechanical energy and generate electrical energy and signals.[9–13]

Currently, a number of polymers have been used and play critical roles as friction and supporting materials in TENGs.[14–16] However, unpredicted damage or performance loss of TENG devices could be induced by the interface friction between different materials and frequent mechanical deformation such as device bending, compressing, stretching, and twisting. Self-healing polymer as novel materials have presented a preferred strategy to solve above problems.[17–19] Self-healing polymers could be classified into intrinsic and extrinsic kinds.[20] Compared with extrinsic systems, intrinsically healable materials are usually flexible and deformable.[21,22] Therefore, intrinsic self-healing polymers induced by supramolecular interaction[23,24] or reversible covalent bonds[25–27] could be ideal materials for self-healing TENGs. The supramolecular systems are physically reversible based on non-covalent interactions with rapidly exchanging.[28–31] Moreover, reversible covalent bonds are relatively stable and robust under ambient conditions, while adaptable under certain stimuli.[32–35]

X. Dai, Dr. Y. Du, Prof. J. Kong
MOE Key Laboratory of Materials Physics and Chemistry in Extraordinary Conditions
Shaanxi Key Laboratory of Macromolecular Science and Technology
School of Science
Northwestern Polytechnical University
Xi'an 710072, P. R. China
E-mail: kongjie@nwpu.edu.cn
Dr. L.-B. Huang, J. Han, Q. Zheng
College of Physics and Optoelectronic Engineering
Shenzhen University
Shenzhen 518060, P. R. China
E-mail: huanglb@szu.edu.cn, huanglbhlb@hotmail.com
Prof. J. Hao
Department of Applied Physics
The Hong Kong Polytechnic University
Hong Kong 999077, P. R. China
E-mail: jh.hao@polyu.edu.hk
The ORCID identification number(s) for the author(s) of this article can be found under https://doi.org/10.1002/adfm.201910723.

DOI: 10.1002/adfm.201910723

Recently, continuous efforts have been made to develop self-healing TENGs. Hao et al. indicated a fully self-healing TENG with disulfide bonds in polydimethylsiloxane-polyurethane (PDMS-PU) and magnetic-assisted electrode.[36] Wang et al. transferred the Ag nanowires and poly(3,4-ethylenedioxythiophene) (Ag-PEDOT) film to imine-containing PDMS to achieve a self-healable, stretchable, and transparent TENG as soft power sources.[37] Pan et al. prepared a near-infrared (NIR) irradiation induced remote TENG through embedding carbon nanotubes (CNTs) in self-healable elastomer and assembling with PDMS.[38] Lai et al. developed an entirely self-healable, highly transparent, and superstretchable TENGs by encapsulating hydrogen-bonding-based hydrogel within metal-ligand-based PDMS.[39] Most of the healable devices are dependent on magnetism, NIR, or even without external stimulation. While the automatically self-healing system might be unstable or take longer time to complete the self-healing process. Additionally, IR radiation from human body is ubiquitous but usually ignored in the use of daily life. Nevertheless, self-healing TENGs as self-powered sensors with real-time repairing feature under skin thermal radiation are merely reported.

In this work, taking advantage of heat converted from human IR radiation, an entirely self-healing and soft TENG based on imine bond and UPy unit (IU-TENG) is prepared and demonstrated as a self-powered sensor to detect human motion. Human skin could emit IR light and radiate heat which can provide an ideal condition to promote self-healing action of polymer. Both the triboelectric layer and electrode could be autonomously self-healable under ambient environments, driven by the dynamic imine bond and quadruple hydrogen bonding UPy motif. With the incorporation of UPy units into imine-based elastomers, the mechanical performances of the materials could be significantly enhanced. The UPy-functionalized multiwalled carbon nanotubes (MWCNTs) have been incorporated into the elastomer and form an electrode with considerable conductivity. Meanwhile, for the devices of multilayered structures, the robust interface bonding has been achieved, because each layer is based on the same healable units. Moreover, the as-prepared IU-TENG device could present high electrical output performances and self-healing as well as shape-tailorable features which could provide promising possibility for the development and applications of TENGs.

2. Results and Discussion

2.1. Design and Performance of Electrification Layer

To fabricate the self-healing and robust TENG stimulated by thermal effect of IR radiation from human body, the self-healable polymer matrix was designed and synthesized, as shown in **Figure 1**a. The self-healing polymer-based networks were

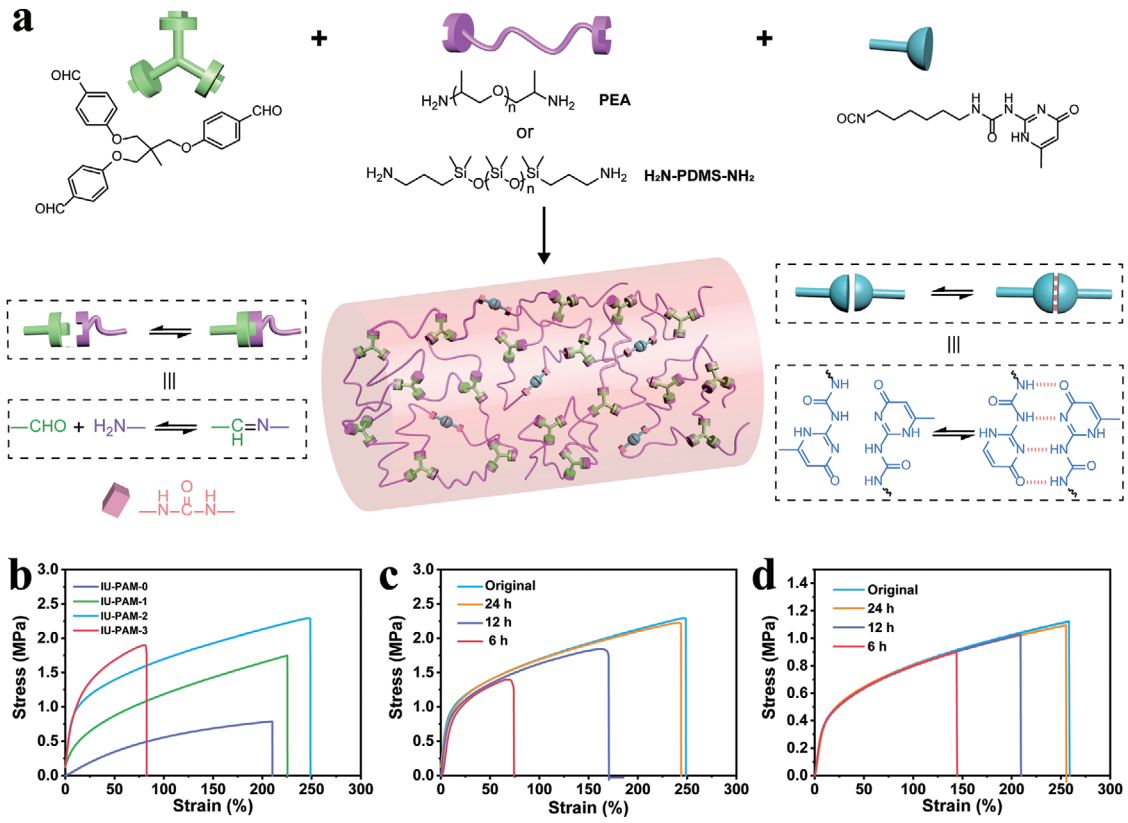

Figure 1. Schematic illustration of the design of self-healing polymeric materials (IU-PAM and IU-PDMS) and mechanical characterization. a) Chemical structures of IU-PAM and IU-PDMS crosslinked by dynamic imine bonds and UPy. b) Stress–strain curves of IU-PAM-0-3 with varying amounts of UPy crosslinks to tune mechanical properties. Stress–strain curves of the original and self-healed c) IU-PAM-2 and d) IU-PDMS specimens after three different healing times from 6 to 12 h and then to 24 h at room temperature.

crosslinked by two kinds of dynamic bonds (imine bond and UPy). Poly(propylene glycol) bis(2-aminopropyl ether) (PEA) or bis(3-aminopropyl) terminated poly(dimethylsiloxane) (H_2N-PDMS-NH_2) was selected as soft segment and it reacts with 2(6-isocyanatohexylaminocarbonylamino)-6-methyl-4[1H] pyrimidinone (UPy-NCO) and 1, 1, 1-tris[(4-formylphenoxy) methyl]ethane (FPME) to obtain flexible and healable polyazomethine (IU-PAM) and poly(dimethylsiloxane) (IU-PDMS) elastomers based on imine and UPy units. A catalytic amount of glacial acetic acid (AcOH) was added to accelerate the reaction between amino and aldehyde groups to form imine bonds (−CH=N−) in the synthesis process. For IU-PAM, a signature peak at 8.23 ppm for imine bonds, and the peaks at 10.13, 11.86, and 13.13 ppm assigned to the protons of UPy units (Figure S2, Supporting Information) were obviously shown in the ^{1}H nuclear magnetic resonance (NMR) spectra (Figure S6, Supporting Information). Furthermore, a new peak at 1645 cm^{-1} confirmed the formation of −CH=N−, and the absence of the isocyanate bands at 2270 cm^{-1} in the Fourier transform infrared spectroscopy (FTIR) spectra of Figure S7 (Supporting Information) revealed that isocyanate groups were completely reacted and UPy moieties were grafted onto polymer chain. Similarly, the data of IU-PDMS in Figures S8 and S9 (Supporting Information) indicated the successful synthesis. A series of healable polyazomethine polymers (IU-PAM-0-3) with different molar ratio were synthesized by varying amounts of UPy and imine moiety. The relative mechanical properties were measured and shown in Figure 1b. With an increase in the contents of UPy, the mechanical performances of polymers were significantly enhanced, which can be ascribed to the rigid structure of UPy segments and the physical crosslinking between polymer chains resulting from the UPy dimers. Served as non-covalent sacrificial bonds, the UPy dimers could dissipate energy through reversible bond rupture during stretching. Meanwhile, the relatively stronger imine bonds were able to maintain the network integrity.[40,41] However, to a certain extent, a mass of UPy can lead to lower flexibility of polymers. Therefore, IU-PAM-2 showed the best mechanical properties with the facture strain of 249% and maxim stress of 2.29 MPa, which was selected to further investigate self-healing performances. Moreover, the ratio of the reactants for IU-PDMS was designed according to that of IU-PAM-2.

The self-healing property was quantitatively investigated by uniaxial tensile tests. Dumbbell-shaped specimens were bisected, and then recombined tightly under different healing conditions. Figure 1c presents the typical stress–strain curve of IU-PAM-2 specimen before and after healing from 6 to 12 h and then to 24 h. When the healing time was over 24 h, the strain and strength of healed samples could restore to 244% and 2.23 MPa, respectively. For IU-PDMS, as shown in Figure 1d, the healed specimens exhibited an elongation at breaking point of 255% and a tensile strength of 1.09 MPa after 24 h, which were almost coincident with original specimens. The healing efficiency was found to enhance as healing time extended. The healing efficiencies of both IU-PAM-2 and IU-PDMS specimens can reach ≈100% after being healed for 24 h, revealing that their mechanical performances could completely revert to the original state and the polymers were provided with excellent self-healing properties. Those results could be contributed to the critical role of the reversible nature of imine bond and UPy motif.[42,43] At the molecular level, the 'mobile phase' existing on or near damaged area could promote intimate contact between scratched surfaces and combine the reactive groups. Meanwhile, the low T_g of IU-PAM-2 (-58.9 °C) and IU-PDMS (−51.0 °C, Figure S10, Supporting Information) enabled the polymer in a high elastic state and enhanced the movement of polymer chain at room temperature, which could facilitate self-healing. The active amino and aldehyde groups generated at the broken interface could reform imine bonds, accompanying with the imine exchange to achieve the integration of fracture surfaces. Moreover, the reformation of UPy dimers through the dissociated hydrogen-bonding could synergistically complete self-healing process.

2.2. Design and Performance of Electrode

The self-healable nanocomposite conductor was prepared by mixing ureidopyrimidinone functionalized MWCNTs (MWCNTs-UPy) with IU-PAM-2, as illustrated in **Figure 2**a. The MWCNTs were functionalized with UPy units (Supporting Information for more details), and subsequently the nanoparticles were added to the solution of polymer containing UPy units (IU-PAM-2). The MWCNTs-UPy/IU-PAM nanocomposite film could be achieved with the evaporation of solvent. The UPy-modified MWCNTs served as a part of physical crosslinks, therefore quadruple hydrogen (UPy dimers) could be formed between particles and polymer chains,[44] reinforcing the compatibility between the MWCNTs-UPy fillers and IU-PAM matrix. From the transmission electron microscopy (TEM) image of MWCNTs-UPy/IU-PAM nanocomposite, it is seen that the nanoparticles are well dispersed in the matrix. The self-healable and conductive capabilities of MWCNTs-UPy/IU-PAM were investigated by connecting the as-prepared sample in a complete circuit composed of a light emitting diode (LED) bulb at first. As shown in Figure 2b, when the sample was cut into two parts, the lighted LED immediately went off. While the two pieces were tightly brought together and maintained at room temperature for 36 h, the LED bulb turned on again as that of the original intact MWCNTs-UPy/IU-PAM films, which indicated the good self-healing ability and electrical conductivity of the nanocomposite. Furthermore, IU-PDMS and MWCNTs-UPy/IU-PAM nanocomposite samples were placed together with fully contact. As shown in Figure 2c, the jointed sample exhibited a good elasticity and bonding strength under bending and twisting, owing to the association–disassociation behaviors of imine bonds and UPy dimers on the surface, which could extend the applications of as-prepared healable polymer materials in flexible devices.

The tensile stress–strain curves of MWCNTs-UPy/IU-PAM for varying healing time at room temperature were systematically researched and shown in Figure 2e. The pristine sample showed a maximum strength of 2.13 MPa and breaking strain of 158%. The specimen healed for 36 h recovered to about 2.12 MPa and 154%, respectively. The healing efficiency reached up to 97%. In addition, it is known that CNTs have strong photothermal properties and they are capable of absorbing NIR.[45,46] The self-healing abilities of MWCNTs-UPy/IU-PAM were further investigated by using an intensity-modulated NIR solid-state diode laser (λ = 808 nm). The images recorded by IR camera in Figure 2d suggested that the surface temperature rose rapidly upon NIR irradiation. A healing efficiency of 88% was observed

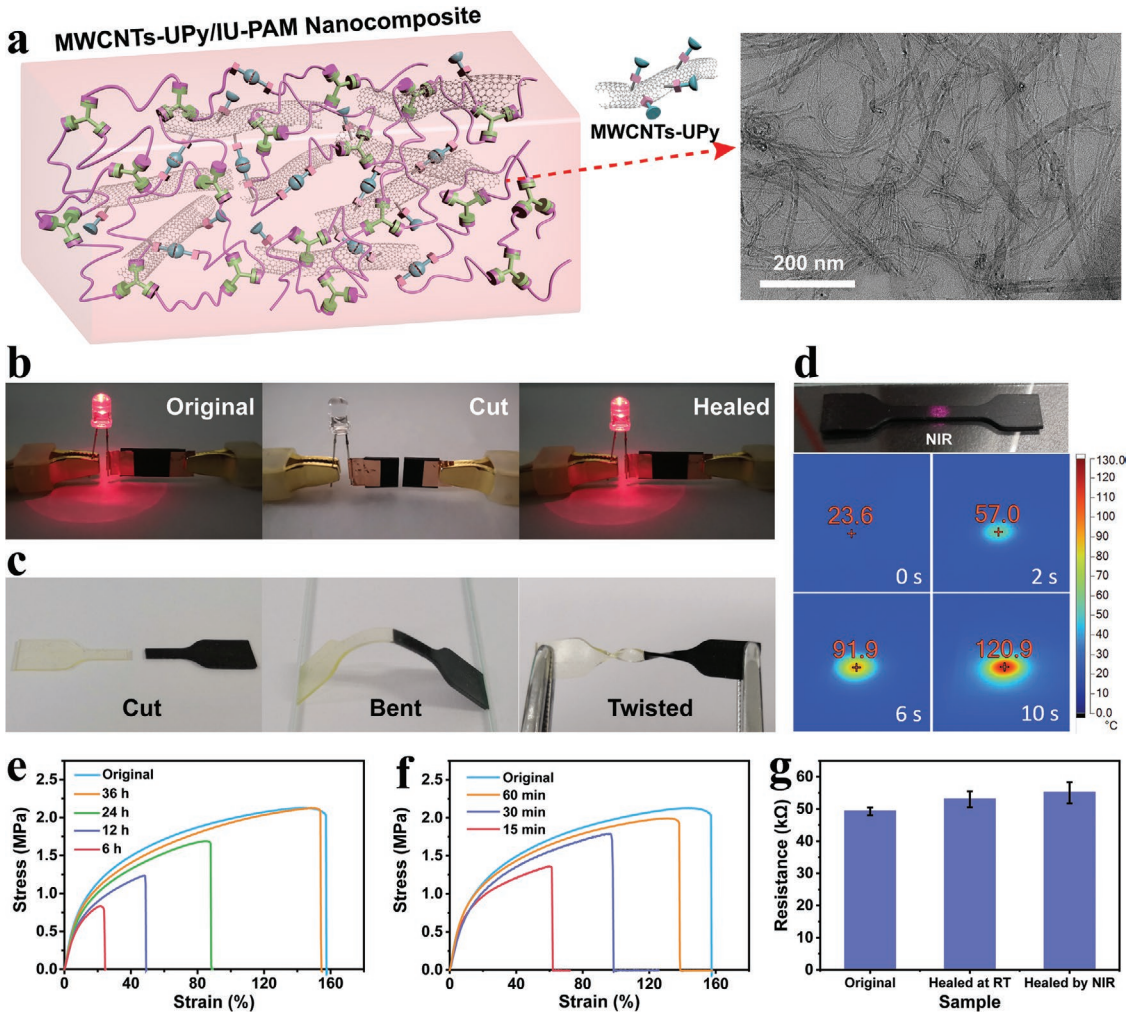

Figure 2. Characterization and performance of the self-healing nanocomposite. a) Illustration of the structure for MWCNTs-UPy/IU-PAM nanocomposite with a TEM image. b) Optical images of MWCNTs-UPy/IU-PAM nanocomposite (the original, after cutting and after healing) in a circuit with an LED bulb. c) Self-healing enabled welding of cut dumbbell between the IU-PDMS and MWCNTs-UPy/IU-PAM. d) Time-lapse FLIR images of MWCNTs-UPy/IU-PAM nanocomposite. Stress–strain curves of the original and self-healed MWCNTs-UPy/IU-PAM after different healing times e) at room temperature and f) under NIR laser irradiation. g) Electrical resistance of the original and self-healed MWCNTs-UPy/IU-PAM nanocomposite.

within 60 min for healing with NIR light exposure (Figure 2f), indicating that the substantial photothermal effect promoted fast healing of wound areas. The electrical conductivities were also quantitatively characterized, as shown in Figure 2g. Not only the original one but also the healed samples with or without NIR irradiation exhibited favorable conductive properties, which could further confirm the excellent self-healing performances of MWCNTs-UPy/IU-PAM.

2.3. Device Fabrication

The fully self-healing IU-TENG device in single-electrode mode was successfully fabricated by sandwiching the MWCNTs-UPy/IU-PAM nanocomposite film between the two IU-PDMS films, as illustrated in **Figure 3**a. The IU-PDMS and MWCNTs-UPy/IU-PAM were regarded as insulating layer and electrode, respectively. A copper tape was attached to the electrode and extended out of the device for electrical connection. Most remarkably, there were robust interface bonding in the IU-TENG device, ensuring the stability and robustness of the device without delamination under frequently deformation. The interface bonding is exceedingly important for the devices with multilayered structure. Without complex physical or chemical post-processing, the good bonding interface was realized. Due to both of the electrode and electrification layer containing dynamic imine bonds and UPy moieties, the different layers could be seamlessly integrated into a single system through the exchange of dynamic bonds at interfaces.

2.4. Device Operation Mechanism

The operation mechanism of the IU-TENG device is schematically described in Figure 3b, originating from the comprehensive actions of contact electrification and electrostatic induction.

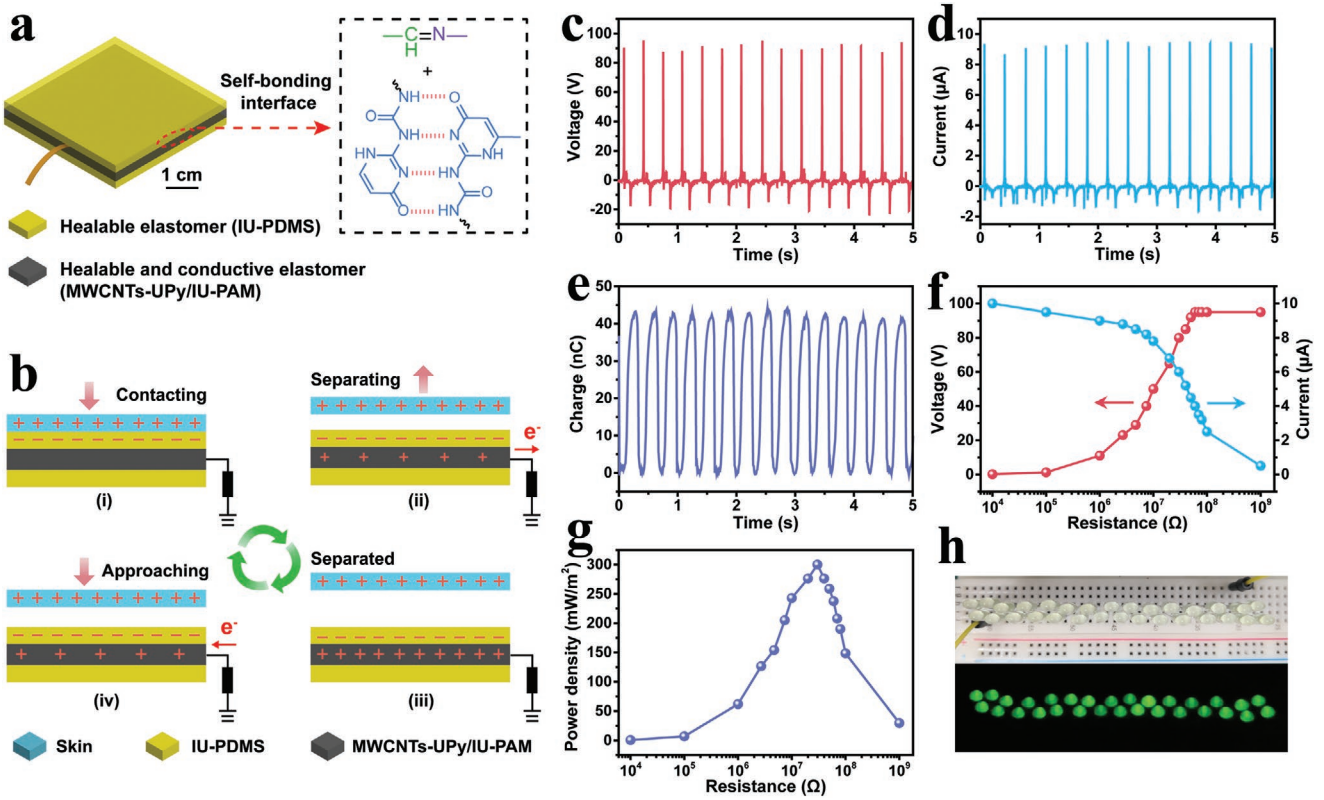

Figure 3. Fabrication and electrical output performance of the IU-TENG. a) Diagram of self-healing IU-TENG. b) Schematic illustration of the working mechanism of the IU-TENG device in single-electrode mode. c) Open-circuit voltage, d) short-circuit current, and e) transferred charge of IU-TENG under contact and separation with a frequency of 3 Hz. f) Output voltage and current versus resistance. g) Variation of power density with external resistance. h) Photograph of thirty green LEDs connected in series driven by the IU-TENG.

When two surfaces of the triboelectric materials (human skin and IU-PDMS) come into contact, electrification could occur at the contact interface, leading to the generation of electrostatic charges with opposite polarities. Owing to the IU-PDMS with higher surface electron affinity compared to skin, the IU-PDMS could be negatively charged. Then, during the separation of the charged surfaces, positive charges could be induced in the CNTs to compensate static charges on the surface of IU-PDMS, and electrons flow from MWCNTs-UPy to the ground, generating an instantaneous electrical current. Upon the complete separation, the induced positive charges in the MWCNTs-UPy are equal to the negative charges in the IU-PDMS, thus there is no potential difference. Once the skin is in contact with IU-PDMS again, the electrons will flow in the opposite direction. By the periodical contact separation between the two triboelectric layers, an alternative current will be continuously generated.

2.5. Device Performance

The electrical output performance of the IU-TENG with the size of 4 cm × 4 cm was investigated and shown in Figure 3c–g. A commercial latex glove was utilized to perform contact-separation motion with IU-TENG under a frequency of 3 Hz. The open-circuit voltage (V_{oc}) could reach a maximum value of about 95 V. The peak short-circuit current (I_{sc}) and transferred charge (Q_{sc}) were about 9.5 μA and 43 nC, respectively. The output voltage and current were resistance-dependent under different external loads. With the increment of loading resistance, the output voltage increased and the current decreased. Correspondingly, the maximum output power density was measured to be about 300 mW m^{-2} when the load resistance was 30 MΩ. As shown in Figure 3h, the IU-TENG was connect with 30 LEDs. The green LEDs were all lighted up when the IU-TENG was pressed by human palm.

The IU-TENG has been demonstrated to exhibit good output electrical properties. During practical usage such as wearable devices on human body, however, the device could suffer from mechanical damage due to periodical external mechanical motion, resulting in poor performance. Fortunately, based on the cooperative self-healing abilities of triboelectric layer and electrode, the whole device could achieve entire self-heal to maintain not only mechanical but also electrical performances. Accordingly, the electric output of the prepared TENGs was systematically investigated under different healing time, temperature, and NIR irradiation. The safety and lifespan of the device were further guaranteed through diverse healing approaches. **Figure 4**a,b presents the V_{oc} and I_{sc} of the original, broken, and self-healed IU-TENG after three different healing times from 3 to 6 h and then to 9 h at 34 °C which is close to the surface temperature of human skin. When the IU-TENG was cut from the middle, both of the V_{oc} and I_{sc} drop by almost half to 46 V

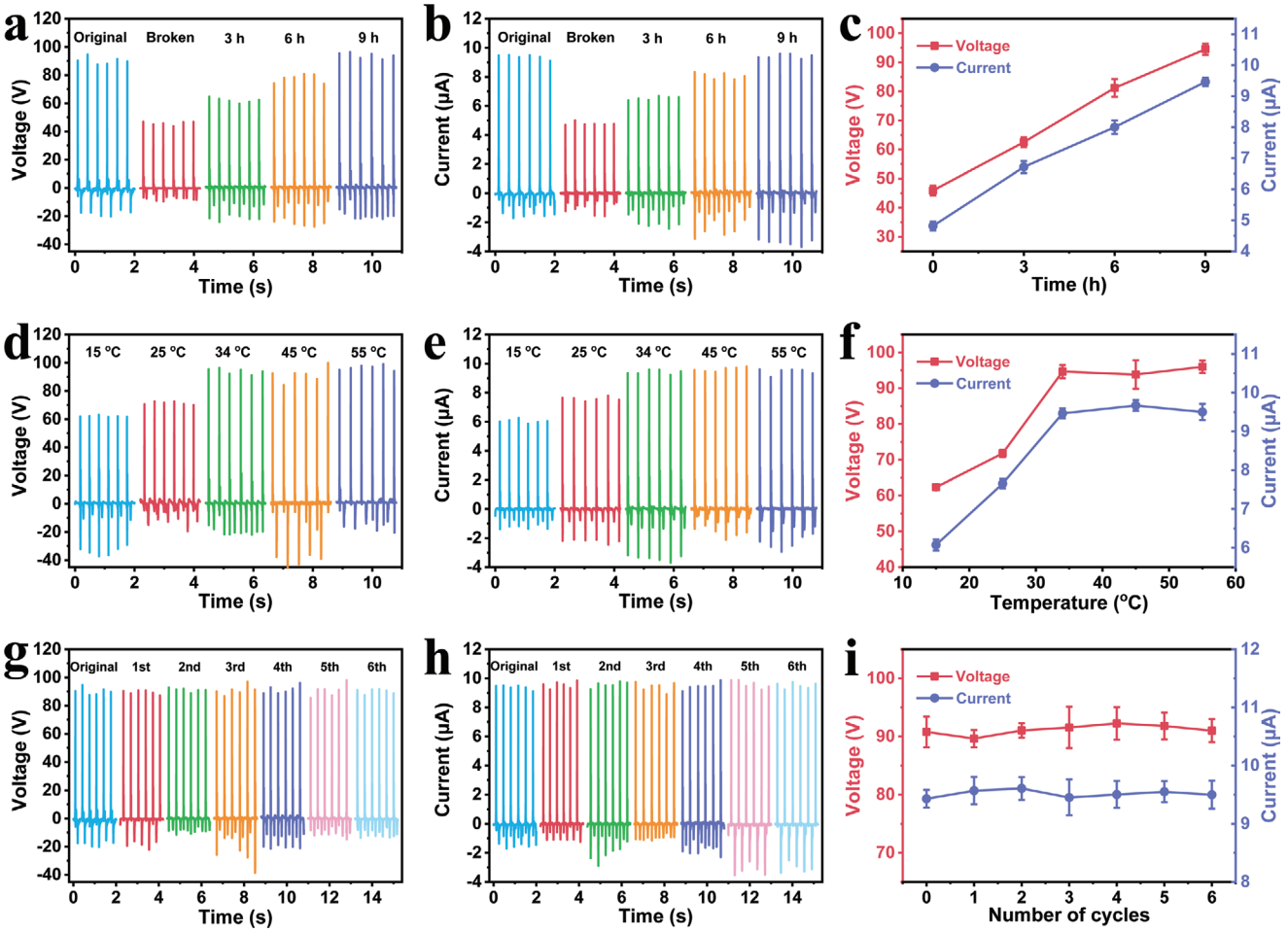

Figure 4. Output characteristics of IU-TENG under varying healing conditions. a) Open-circuit voltage and b) short-circuit current of the original, broken, and self-healed IU-TENG after three different healing times from 3 to 6 h and then to 9 h at 34 °C. c) Voltage and current change of IU-TENG after different healing times at 34 °C. d) Open-circuit voltage and e) short-circuit current of self-healed IU-TENG at different temperatures (15, 25, 34, 45, and 55 °C) for 9 h. f) Voltage and current change of IU-TENG at different healing temperatures for 9 h. g) Open-circuit voltage and h) short-circuit of the original and self-healed IU-TENG after one to four cycles under NIR irradiation. i) Voltage and current change of IU-TENG after healing under NIR irradiation for several cycles (0 represent the original).

and 4.8 μA, respectively, attributed to the decrease of effective contact areas. Then, the broken surfaces were brought into full contact. From Figure 4c, it was found that the time-dependent healing process was completed after 9 h at 34 °C. The V_{oc} and I_{sc} of self-healed IU-TENG at different temperatures (15, 25, 34, 45, and 55 °C) for 9 h are exhibited in Figure 4d,e. The healing process was also temperature-dependent, as shown in Figure 4f. Above 34 °C, the whole recovery time of device might last about 9 h. While the temperature was lower than 34 °C, the repair time of device could be elongated due to relatively low molecular activity. Moreover, the IU-TENG could perform fast self-repair under assistance of NIR irradiation for 30 min (Figure 4g,h). The repeated self-healing feature of IU-TENG was further investigated as shown in Figure 4i. After broken and repaired for six times, the V_{oc} and I_{sc} of self-healed IU-TENG remained almost same values with original device. It was worth noting that under NIR irradiation, the temperature of MWCNTs-UPy/IU-PAM rapidly rose to 120 °C (Figure 2d), indicating that the IU-TENG exhibited stable output performance over a wide temperature range. Those results presented that, under different temperature or NIR irradiation, the electrical performance of IU-TENG device could restore to its original state.

Benefiting from the excellent self-healing properties of IU-TENG, the as-prepared device was endowed with shape-tailorable capability, which extend TENGs to satisfy different applications with various shapes. In our previous work, shape-tailorable TENGs have been fabricated using healable polymer, magnetic balls, and cubes.[36] The shape-tailorability of TENG device was limited by the rigid magnetic components. By utilization of flexible self-healing and conductive materials, we further enhance the shape-tailorability of TENG which could be tailored into arbitrary shapes. As shown in **Figure 5**a, the original IU-TENG was cut into different shapes including arc, square, and triangle shape which were utilized to assemble TENG in different shapes (shapes 1–3). The V_{oc} and I_{sc} of the original, after cutting, and shapes 1–3 after healing were presented in Figure 5b. After cutting, contact areas of TENG decreased, leading to the decrement of the V_{oc} and I_{sc}. Once the pieces were assembled into an intact

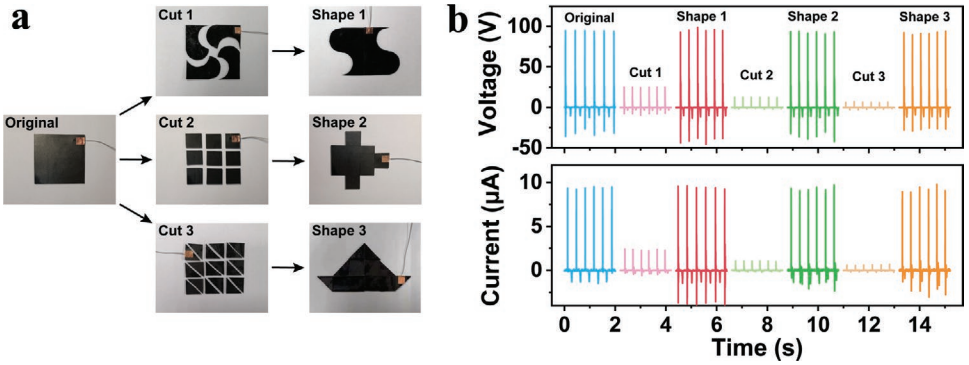

Figure 5. Shape-tailorable performance of IU-TENG. a) Optical images of the tailorable process for the IU-TENG (the original, after cutting into 4, 9, and 18 pieces, and shapes 1–3 after healing). b) Open-circuit voltage and short-circuit current of the original, cut and re-shaped IU-TENG.

shape for self-healing, the V_{oc} and I_{sc} recover to about 95 V and 9.4 μA, respectively. All of the re-shaped IU-TENGs exhibited excellent output electrical performances, which were same as that of original device. These excellent results demonstrated the outstanding shape-tailorability of IU-TENG.

2.6. Self-Powered Sensor

Followed by the above systematical investigations of output performance, self-healing capability, and tailorability, IU-TENG could be utilized as self-powered sensor to detect human motion. Structure of TENG device based on IU-TENG with 40 mm × 20 mm is designed and schematically depicted in **Figure 6**a. The bottom layer (IU-PDMS) is an insulator to separate human body from the electrode. The middle electrode (MWCNTs-UPy/IU-PAM) is tightly attached to the bottom one through self-bonding, driven by the reversible exchange of imine bonds and UPy moieties. Additionally, the middle electrode and top layer (IU-PDMS) served as electrification layers, which were separated by two small spacers (IU-PDMS) to realize the contact-separation motions under the external

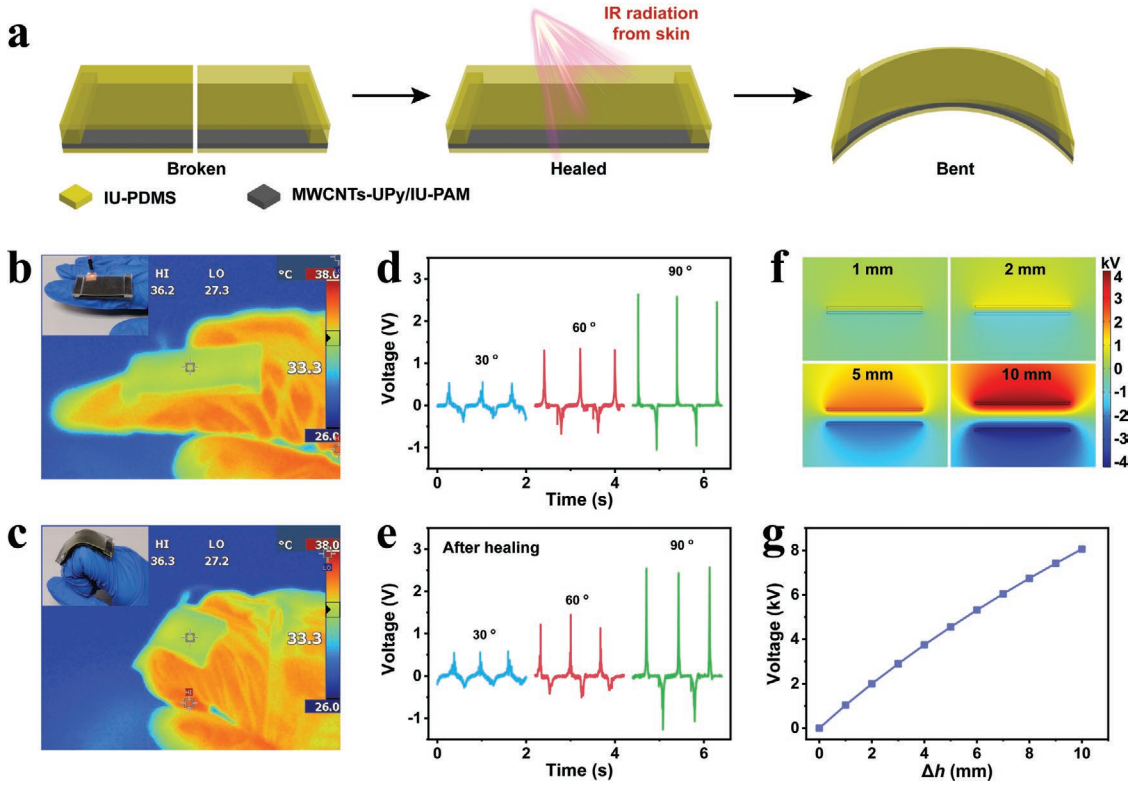

Figure 6. Demonstration of the self-healable TENG for human motion detection. a) Schematic diagrams of the self-healing TENG via IR radiation from skin. Thermal images with inset optical images of b) the original and c) bent TENG on the finger. Open-circuit voltage responses when bending the finger joint at different angles (30°, 60°, and 120°) of d) the original and e) self-healed TENG. f, g) Numerical calculation of the potential distribution of the TENG at varying gap between IU-PDMS and MWCNTs-UPy/IU-PAM nanocomposite by using COMSOL software.

force. The as-fabricated flexible TENG device could be used as a self-powered finger-joint motion sensor, which could be properly attached to the finger in a straight state (Figure 6b) and subjected to bend (Figure 6c). With the bending angle periodically changing from 30° to 60° and then to 90°, the output V_{oc} was 0.6, 1.4, and 2.7 V, respectively (Figure 6d). As the bending angle increased, the contact area of two triboelectric layers was enlarged, leading to rising the V_{oc} of the TENG sensor simultaneously. Therefore, the change of bending angle in the finger-joint motion can be monitored via the change of open-circuit voltage. In addition, the gap between the triboelectric layers had a significant influence on the output performance. The potential distribution of two triboelectrically charged materials under open-circuit condition are simulated by COMSOL (Figure 6f). From the simulation results, it was obviously observed that the open-circuit voltage was proportional to the gap between triboelectric layers, indicating the detection signal could be enhanced through enlarging the gap (Figure 6g).

During device operation, the as-prepared self-powered sensor might be damaged or destroyed by frequent bending and friction. Providentially, the broken device on the finger could be timely self-healed based on thermal effect of IR radiation from skin. In addition, if the device was taken off from body, NIR could be utilized to facilitate fast self-healing processes. Multiple repairing methods can ensure and enhance reliability and safety of device. Most of human body heat is dissipated as IR radiation, and the reported IR emittance of skin is 0.98.[47] As a result, human skin can be considered as natural IR emitter. At the skin temperature of 34 °C, IR radiation from human body is mainly in the range of 8–14 μm with the peak emission at the wavelength of 9.5 μm.[47,48] Under IR light ranging from 0.5 to 3 μm, the temperature of MWCNTs-UPy/IU-PAM rose rapidly, resulting from the good photothermal effect of MWCNTs-UPy (**Figure 7**a–c). Moreover, the measured IR emittance of MWCNTs-UPy/IU-PAM was 0.91 in the range of 1.5–21 μm, further indicating the as-prepared TENG device could efficiently absorb the IR radiation. As the TENG device was attached to finger, the temperature of materials increased under the IR radiation from human body, which could promote self-healing (Figure 6a–c). The device was scratched, and assembled together in full contact, and then put on skin. After complete healing, the device could still be subjected to bend from 30° to 90°, with the V_{oc} increasing from 0.6 to 2.6 V, which was almost consistent with that of the original one (Figure 6e). The results suggested that the as-fabricated TENG device served as a self-powered sensor exhibited excellent self-healing performance under the IR radiation from human body.

3. Conclusion

In summary, entirely self-healing, flexible, and tailorable TENGs with robust interface bonding have been developed for potential applications in self-powered sensors. Attributed to both electrode and electrification layer containing the dynamic imine bonds and UPy moieties, the different layers were seamlessly integrated into a single system through the exchange of dynamic bonds at interfaces, ensuring the TENG device mechanically robust and electrically stable. The UPy units were intentionally incorporated into imine-based elastomers to improve the mechanics performance and synergistically motivate self-healing. By modifying the MWCNTs with UPy motif, a good compatibility between nanofillers and polymer segments was achieved to facilitate the reconfiguration of conductive networks during repair. Meanwhile, our designed and synthesized materials (IU-PDMS and MWCNTs-UPy/IU-PAM) and the assembled IU-TENG device exhibited intrinsically unique self-healing feature driven by the reversible bond-based molecular interconnects, with mechanical and electrical properties well recovered. Furthermore, the self-healing TENG could be easily tailored and implemented on self-powered devices to detect human motions, with IR thermal radiation from human skin effectively promoting self-healing to realize timely recovery after damage. This can be the foundation of integration design of self-healing and self-powered soft devices for reliability, safety, and environmental sustainability.

4. Experimental Section

Materials: 2-Amino-4-hydroxy-6-methylpyrimidine (MIC, 98.0%), hexamethylene diisocyanate (HDI, 99.0%), PEA (M_n = 2000) were purchased from Aladdin. H_2N-PDMS-NH_2 (M_n = 5000–7000) were purchased from Gelest. Amino-functionalized MWCNTs (MWCNTs-NH_2, average diameter of 8–15 nm, length of 50 um) were purchased from Nanjing XFNANO Materials Tech. Co. Ltd. FPME were prepared via previously reported procedures.[32] All reagents were utilized as supplied without further purification.

Synthesis of UPy-NCO: The synthesis was carried out according to the reported procedures,[49] as shown in Figure S1 (Supporting Information). MIC (1.25g, 0.01 mol) and HDI (11.44 mL, 0.068mol) were mixed in

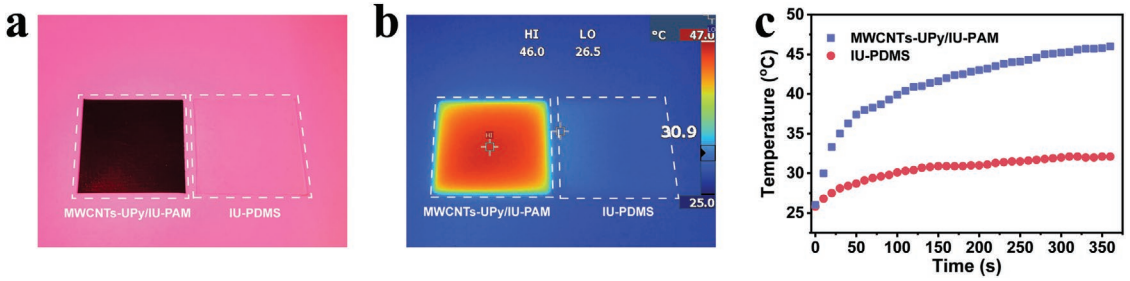

Figure 7. IR absorption characteristics of MWCNTs-UPy/IU-PAM and IU-PDMS. a) Optical image and b) thermal image of MWCNTs-UPy/IU-PAM left) and IU-PDMS right) under IR lamp. c) Temperature rise of samples under IR irradiation for 360 s.

a flask equipped with a reflux condenser with stirring at 100 °C under nitrogen atmosphere for 24 h. After cooling to room temperature, pentane was poured into the mixture. The precipitate was collected and dried at 50 °C in vacuum for overnight.

Preparation of MWCNTs-UPy: As shown in Figure S3 (Supporting Information), to a solution of UPy-NCO (0.4 g) in 50 mL of anhydrous N, N-dimethylformamide (DMF), MWCNTs-NH_2 (0.4 g) was added and ultrasonicated for 30 min. The mixture was kept at 80 °C to continue the reaction under nitrogen atmosphere for 24 h with vigorously mechanical stirring. The MWCNTs-UPy product was separated from the suspension and washed with DMF and dichloromethane, and dried at 60 °C under vacuum oven for 24 h.

Preparation of IU-PAM: For IU-PAM-2 sample preparation, PEA 2000 (2.7 g, 1.35 mmol) and UPy-NCO (0.135 g, 0.45 mmol) were dissolved in 8 mL of DMF. The mixture was heated at 80 °C for 6 h. After cooling to room temperature, FPME (0.342g, 0.75 mmol) and AcOH (25 µL) were added with stirring for 12 h. After reaction, the solvent was evaporated and dried in an oven overnight. Then, the product (3 g) was dissolved in 15 mL of chloroform ($CHCl_3$). The solution was poured into a Teflon dish and allowed to slowly evaporate at room temperature overnight. Finally, the resulting film was dried in a vacuum oven at 60 °C for 24 h. The same procedure was used to prepare films based on other IU-PAMs (Table S1, Supporting Information).

Preparation of MWCNTs-UPy/IU-PAM Nanocomposite: IU-PAM-2 (3 g) was dissolved in 15 mL of $CHCl_3$, followed by adding the synthesized MWCNTs-UPy (0.158 g, 5 wt%). The mixture was ultrasonicated for 30 min, and transferred into a Teflon mould, which was allowed to slowly evaporate solvent at room temperature. The obtained film was dried in an oven for 24 h.

Preparation of IU-PDMS: UPy-NCO (0.06 g, 0.2 mmol) was added to the solution of H_2N-PDMS-NH_2 (3 g, 0.6 mmol) in 15 mL of $CHCl_3$, and the mixture was heated at 60 °C under reflux for 6 h. After the solution was cooled to room temperature, FPME (0.152g, 0.333 mmol) was added and stirred overnight. The solution was casted on a Teflon mold and dried at room temperature for 24 h followed by drying at 60 °C for 24 h in a vacuum oven.

Fabrication of IU-TENG: The prepared MWCNTs-UPy/IU-PAM nanocomposite and IU-PDMS films (0.5 mm thick) were cut into squares (40 mm × 40 mm) with a razor, respectively. The self-healing TENG device was fabricated by sandwiching the MWCNTs-UPy/IU-PAM nanocomposite layer between the two IU-PDMS layers with a copper tape attached to the nanocomposite for the convenience of measurement.

Fabrication of Self-Healing TENG Sensor: The prepared MWCNTs-UPy/IU-PAM nanocomposite and IU-PDMS films (0.5 mm thick) were cut into rectangles (40 mm × 20 mm) with a razor, respectively. A piece of MWCNTs-UPy/IU-PAM nanocomposite film was placed on top of the IU-PDMS film. Then, another layer of IU-PDMS with the spacer (2 mm thick) was attached to the MWCNTs-UPy/IU-PAM through self-bonding.

Characterization: NMR analyses were conducted on a Bruker Avance 400 instrument. FTIR tests were performed on a Nicolet iS10 IR spectrometer (Thermo Scientific, USA). The mechanical tensile tests were performed using an Instron 3342 universal tester with a stretching speed of 20 mm min^{-1} according to ISO37-4. The healing efficiency was defined as the ratio of elongation at break of healed specimens to that of original specimens. Differential scanning calorimetry (DSC) was performed using a Mettler Toledo DSC 1 instrument with the heating rate of 10 °C min^{-1}. Thermogravimetric analysis were recorded using an STA, 449C Jupiter instrument under an argon atmosphere with a heating rate of 10 K min^{-1}. TEM (FEI Talos F200X) was operated at an accelerating voltage of 200 kV. Resistance measurements were conducted on Keithley 2450 source meter. The output voltage was measured by an oscilloscope (LeCroy WaveSurfer 62Xs 600MHz 2.5 GS/s). The output current was characterized by a low noise current amplifier (Stanford Research Systems, SR570). The charge transfer was measured using an electrometer (Keithley 6514). IR thermal images were recorded by a Fluke Ti300 IR imager. IR emittance was performed using an AZUP ET100 IR emissivity meter in the range of 1.5–21 µm.

Supporting Information

Supporting Information is available from the Wiley Online Library or from the author.

Acknowledgements

X.D. and L.-B.H. contributed equally to this work. The research was financially supported by the National Natural Science Foundation of China through grants (21875190 and 51973119), Shaanxi Natural Science Funds for Distinguished Young Scholars (2018JC-008), the Natural Science Foundation of Guang Dong Province (2018A0303130060 and 2019A1515011566), and the Science and Technology Innovation Commission of Shenzhen City (JCYJ20170818101245583).

Conflict of Interest

The authors declare no conflict of interest.

Keywords

infrared radiation, reversible bonds, self-healing, self-powered sensors, triboelectric nanogenerators

Received: December 26, 2019
Revised: February 3, 2020
Published online:

[1] Z. L. Wang, *Adv. Mater.* **2012**, *24*, 280.
[2] H. Chen, Y. Song, X. Cheng, H. Zhang, *Nano Energy* **2019**, *56*, 252.
[3] S. S. Kwak, H.-J. Yoon, S.-W. Kim, *Adv. Funct. Mater.* **2019**, *29*, 1804533.
[4] S. Park, S. W. Heo, W. Lee, D. Inoue, Z. Jiang, K. Yu, H. Jinno, D. Hashizume, M. Sekino, T. Yokota, K. Fukuda, K. Tajima, T. Someya, *Nature* **2018**, *561*, 516.
[5] F. R. Fan, W. Tang, Z. L. Wang, *Adv. Mater.* **2016**, *28*, 4283.
[6] Z. L. Wang, J. Chen, L. Lin, *Energy Environ. Sci.* **2015**, *8*, 2250.
[7] M. Xu, T. Zhao, C. Wang, S. L. Zhang, Z. Li, X. Pan, Z. L. Wang, *ACS Nano* **2019**, *13*, 1932.
[8] G. Yao, D. Jiang, J. Li, L. Kang, S. Chen, Y. Long, Y. Wang, P. Huang, Y. Lin, W. Cai, X. Wang, *ACS Nano* **2019**, *13*, 12345.
[9] X. Li, G. Xu, X. Xia, J. Fu, L. Huang, Y. Zi, *Nano Energy* **2019**, *56*, 40.
[10] Y. Zi, J. Wang, S. Wang, S. Li, Z. Wen, H. Guo, Z. L. Wang, *Nat. Commun.* **2016**, *7*, 10987.
[11] X.-S. Zhang, M. Han, B. Kim, J.-F. Bao, J. Brugger, H. Zhang, *Nano Energy* **2018**, *47*, 410.
[12] G. Liu, J. Chen, Q. Tang, L. Feng, H. Yang, J. Li, Y. Xi, X. Wang, C. Hu, *Adv. Energy Mater.* **2018**, *8*, 1703086.
[13] L.-B. Huang, W. Xu, G. Bai, M.-C. Wong, Z. Yang, J. Hao, *Nano Energy* **2016**, *30*, 36.
[14] J. H. Lee, R. Hinchet, S. K. Kim, S. Kim, S.-W. Kim, *Energy Environ. Sci.* **2015**, *8*, 3605.
[15] X. Cao, M. Zhang, J. Huang, T. Jiang, J. Zou, N. Wang, Z. L. Wang, *Adv. Mater.* **2018**, *30*, 1704077.
[16] L.-B. Huang, G. Bai, M.-C. Wong, Z. Yang, W. Xu, J. Hao, *Adv. Mater.* **2016**, *28*, 2744.
[17] T. P. Huynh, P. Sonar, H. Haick, *Adv. Mater.* **2017**, *29*, 1604973.
[18] D. Chen, D. Wang, Y. Yang, Q. Huang, S. Zhu, Z. Zheng, *Adv. Energy Mater.* **2017**, *7*, 1700890.

[19] M. D. Bartlett, M. D. Dickey, C. Majidi, *NPG Asia Mater.* **2019**, *11*, 1.
[20] S. Y. An, D. Arunbabu, S. M. Noh, Y. K. Song, J. K. Oh, *Chem. Commun.* **2015**, *51*, 13058.
[21] J. Kang, J. B. H. Tok, Z. Bao, *Nat. Electron.* **2019**, *2*, 144.
[22] L. M. Zhang, Y. He, S. Cheng, H. Sheng, K. Dai, W. J. Zheng, M. X. Wang, Z. S. Chen, Y. M. Chen, Z. Suo, *Small* **2019**, *15*, 1804651.
[23] Y. Yang, M. W. Urban, *Adv. Mater. Interfaces* **2018**, *5*, 1800384.
[24] X. Yan, F. Wang, B. Zheng, F. Huang, *Chem. Soc. Rev.* **2012**, *41*, 6042.
[25] R. J. Wojtecki, M. A. Meador, S. J. Rowan, *Nat. Mater.* **2011**, *10*, 14.
[26] W. Zou, J. Dong, Y. Luo, Q. Zhao, T. Xie, *Adv. Mater.* **2017**, *29*, 1606100.
[27] P. Chakma, D. Konkolewicz, *Angew. Chem., Int. Ed.* **2019**, *58*, 9682.
[28] X. Wu, J. Wang, J. Huang, S. Yang, *ACS Appl. Mater. Interfaces* **2019**, *11*, 7387.
[29] M. Liu, P. Liu, G. Lu, Z. Xu, X. Yao, *Angew. Chem., Int. Ed.* **2018**, *57*, 11242.
[30] J. Chen, Q. Peng, T. Thundat, H. Zeng, *Chem. Mater.* **2019**, *31*, 4553.
[31] C.-H. Li, C. Wang, C. Keplinger, J.-L. Zuo, L. Jin, Y. Sun, P. Zheng, Y. Cao, F. Lissel, C. Linder, X.-Z. You, Z. Bao, *Nat. Chem.* **2016**, *8*, 618.
[32] X. Dai, Y. Du, J. Yang, D. Wang, J. Gu, Y. Li, S. Wang, B. B. Xu, J. Kong, *Compos. Sci. Technol.* **2019**, *174*, 27.
[33] Z. Zou, C. Zhu, Y. Li, X. Lei, W. Zhang, J. Xiao, *Sci. Adv.* **2018**, *4*, eaaq0508.
[34] Z. Wei, D. M. Lewis, Y. Xu, S. Gerecht, *Adv. Healthcare Mater.* **2017**, *6*, 1700523.
[35] A. Rekondo, R. Martin, A. Ruiz de Luzuriaga, G. Cabanero, H. J. Grande, I. Odriozola, *Mater. Horiz.* **2014**, *1*, 237.
[36] W. Xu, L.-B. Huang, J. Hao, *Nano Energy* **2017**, *40*, 399.
[37] J. Sun, X. Pu, M. Liu, A. Yu, C. Du, J. Zhai, W. Hu, Z. L. Wang, *ACS Nano* **2018**, *12*, 6147.
[38] Q. Guan, Y. Dai, Y. Yang, X. Bi, Z. Wen, Y. Pan, *Nano Energy* **2018**, *51*, 333.
[39] Y.-C. Lai, H.-M. Wu, H.-C. Lin, C.-L. Chang, H.-H. Chou, Y.-C. Hsiao, Y.-C. Wu, *Adv. Funct. Mater.* **2019**, *29*, 1904626.
[40] J. A. Neal, D. Mozhdehi, Z. Guan, *J. Am. Chem. Soc.* **2015**, *137*, 4846.
[41] H. Zhang, Y. Wu, J. Yang, D. Wang, P. Yu, C. T. Lai, A.-C. Shi, J. Wang, S. Cui, J. Xiang, N. Zhao, J. Xu, *Adv. Mater.* **2019**, *31*, 1904029.
[42] Y. Song, Y. Liu, T. Qi, G. L. Li, *Angew. Chem., Int. Ed.* **2018**, *57*, 13838.
[43] F. Song, Z. Li, P. Jia, M. Zhang, C. Bo, G. Feng, L. Hu, Y. Zhou, *J. Mater. Chem. A* **2019**, *7*, 13400.
[44] T. T. T. Myllymäki, L. Lemetti, Nonappa, O. Ikkala, *ACS Macro Lett.* **2017**, *6*, 210.
[45] C.-R. Chen, H. Qin, H.-P. Cong, S.-H. Yu, *Adv. Mater.* **2019**, *31*, 1900573.
[46] W. Pu, D. Fu, Z. Wang, X. Gan, X. Lu, L. Yang, H. Xia, *Adv. Sci.* **2018**, *5*, 1800101.
[47] L. Cai, A. Y. Song, W. Li, P.-C. Hsu, D. Lin, P. B. Catrysse, Y. Liu, Y. Peng, J. Chen, H. Wang, J. Xu, A. Yang, S. Fan, Y. Cui, *Adv. Mater.* **2018**, *30*, 1802152.
[48] A. Hazarika, B. K. Deka, C. Jeong, Y.-B. Park, H. W. Park, *Adv. Funct. Mater.* **2019**, *29*, 1903144.
[49] B. J. B. Folmer, R. P. Sijbesma, R. M. Versteegen, J. A. J. van der Rijt, E. W. Meijer, *Adv. Mater.* **2000**, *12*, 874.